Electrochimica Acta 97 (2013) 278–288

Contents lists available at SciVerse ScienceDirect

Electrochimica Acta

journal homepage: www.elsevier.com/locate/electacta

Effect of convective mass transfer on lead-acid battery performance

Ali Ghorbani Kashkooli [a], Siamak Farhad [b,*], Alan S. Fung [b], Zhongwei Chen [c]

[a] Faculty of Industrial and Mechanical Engineering, Qazvin Branch, Islamic Azad University, Nokhbegan Blvd., Qazvin 34185-1416, Iran
[b] Department of Mechanical and Industrial Engineering, Ryerson University, 350 Victoria Street, Toronto, Ontario, Canada M5B 2K3
[c] Department of Chemical Engineering, University of Waterloo, 200 University Avenue West, Waterloo, Ontario, Canada N2L 3G1

ARTICLE INFO

Article history:
Received 27 December 2012
Received in revised form 22 February 2013
Accepted 23 February 2013
Available online 13 March 2013

Keywords:
Lead-acid battery modeling
Convective mass transfer
Specific energy and power
State of charge
Salt concentration in electrolyte

ABSTRACT

The effect of convective mass transfer in electrolyte solution on the lead-acid battery performance is studied through computer simulation. For this purpose, the battery performance predicted from a model that considers full mass transport equations is compared to that predicted from a model that considers only mass transport due to diffusion and migration. To generalize the results, a sensitivity analysis is conducted to elucidate the dependency of the effect of convective mass transfer to the electrode thickness, electrode initial porosity, and initial acid concentration. In the range of the battery design and operating conditions investigated, the convective mass transfer may affect the battery specific power and energy up to 1%, the state of charge up to 2.4%, and the salt concentration in the positive electrode up to 50%.

1. Introduction

The lead-acid battery is a rechargeable electrical energy storage device with a broad-range of applications in automotive industry, back-up power supplies, and load leveling systems. A simple and accurate mathematical model plays a crucial role in optimum designing this battery for these and new applications. Today's battery models provide a suitable platform to investigate physical and electrochemical processes occurring inside this battery at various operating and design conditions. In literature, many mathematical models have been published on the lead-acid battery [1–4]. The first ones using porous electrode theory emerged in 1960s and 1970s [5,6]. A complete single cell model to describe battery discharge behavior was suggested by Tiedemann and Newman in 1979 [7]. In 1987, Gu et al. [8] improved the battery model to predict the battery performance at both charge and discharge processes. By employing mathematical models, the study of various battery/cell designs and their impact on the cell performance became feasible. Ekdunge and Simonsson [9] studied capacity limiting process by varying the initial acid concentration in electrolyte using mathematical modeling. Dimpault-Darcy et al. [10] examined effects of various design parameters such as electrode thicknesses, electrode conductivity, and operating temperature on battery performance. Kim et al. [11] studied the effect of various initial porosities and cathodic transfer coefficients on the flooded cell discharge behavior.

In most of the models developed so far, convection, diffusion and migration mass transfer phenomena have been taken into account. In some models, the effect of convective mass transfer is neglected to simplify the model [12]; however, there is no evidence to address the limitations and impacts of this simplification on the modeling results. If the convective term can be neglected from mass transfer equations, an improvement in terms of the model simplification and reduction in the computational cost can be yielded; and the model will be more applicable for real-time performance prediction purposes. The aim of this study is to investigate the effect of convective mass transfer phenomenon on the lead-acid battery performance. For this purpose, a comprehensive study is conducted at various battery design and operating conditions to quantify the effect of this phenomenon on the battery performance. In this study, COMSOL Multyphysics 4.2 was employed to simulate the lead-acid battery.

2. Modeling and computer simulation

The mathematical model employed to simulate lead-acid battery is based on the model presented in Refs. [7,8,13,14]. In this model, the mass and charge transport equations are developed for each components of the cell structure, including the positive porous lead dioxide electrode, electrolyte reservoir, porous separator, and negative porous spongy lead electrode (see Fig. 1). It is assumed that the cell is isothermal and homogenous, pores in electrodes are completely filled with electrolyte, electrolyte is a concentrated solution of sulfuric acid that dissociates in water into positively charged hydrogen ion, H^+, and negatively charged hydrogen sulfate,

* Corresponding author. Tel.: +1 519 888 4567x31624.
E-mail address: sfarhad@uwaterloo.ca (S. Farhad).

0013-4686/$ – see front matter
http://dx.doi.org/10.1016/j.electacta.2013.02.116

Nomenclature

a_{max}	maximum active surface area (m^2)
c	electrolyte concentration ($mol\,cm^{-3}$)
C_{dl}	electrical double layer capacitance ($F\,m^{-2}$)
D	diffusion coefficient ($m^2\,s^{-1}$)
E	specific energy ($Wh\,kg^{-1}$)
ex	exponent on porosity
exm	exponent on porosity due to the tortuosity effect
F	Faraday's constant, 96487 ($C\,mol^{-1}$)
h	cell height (m)
i	current density ($A\,m^{-2}$)
I	total applied current density to the cell ($A\,m^{-2}$)
i_0	exchange current density ($A\,m^{-2}$)
l	thickness (m)
m	molality of the electrolyte ($mol\,kg^{-1}$)
M	molecular weight ($g\,mol^{-1}$)
n	number of electrons involved in the reaction
$\dot{N}''_x$	rate of molar flux ($mol\,s^{-1}\,m^{-2}$)
P	specific power ($W\,kg^{-1}$)
R	rate of electrochemical reaction ($mol\,s^{-1}\,m^{-3}$)
s	stoichiometric coefficient
soc	electrode state of charge
t	time (s)
T	temperature (K)
t^0_+	transference number of H^+ with respect to the solvent
U^0	standard electrode potential (V)
$\bar{V}$	convective volume average velocity of solution ($m\,s^{-1}$)
$\bar{v}_e$	partial molar volume of H_2SO_4 ($m^3\,mol^{-1}$)
$\bar{v}_0$	partial molar volume of HO_2 ($m^3\,mol^{-1}$)
W	cell width (m)
x	spatial coordinate along the thickness of the cell
z	charge number

Greek letters

α_a	anodic transfer coefficient
α_c	cathodic transfer coefficient
β	current collector to electrode weight ratio
γ	exponent on concentration
ε	porosity
ζ	morphology parameter in kinetics
κ	electrolyte conductivity ($S\,m^{-1}$)
υ	dissociation coefficient
ρ	density ($kg\,m^{-3}$)
σ	electronic conductivity ($S\,m^{-1}$)
ϕ	electric potential (V)
ω	mass per unit area of the cell ($kg\,m^{-2}$)

Subscripts

+	positive electrode
−	negative electrode
0	zero charge/solvent
1	electronic
2	ionic
e	electrolyte
eff	effective
i	positive or negative charge
init	initial
max	fully charged
ref	reference
sep	separator
pos	positive electrode
neg	negative electrode
res	reservoir

Superscripts

+	length plus epsilon
−	length mines epsilon

HSO_4^-. The following electrochemical reactions take place inside the cell during the discharge and charge processes [15]:

$$\text{Positive electrode}: \quad PbO_2 + HSO_4^- + 3H^+ + 2e^- \rightleftharpoons PbSO_4 + 2H_2O \tag{R1}$$

$$\text{Negative electrode}: \quad Pb + HSO_4^- \rightleftharpoons PbSO_4 + H^+ + 2e^- \tag{R2}$$

In this study, the emphasis is on the mass transfer equation in the electrolyte solution in the negative electrode, reservoir, separator and positive electrode. In the electrolyte solution, the one-dimensional mass transfer equation is expressed as follows [16]:

$$\frac{\partial(\varepsilon c)}{\partial t} = -\frac{\partial(\dot{N}''_{x,i})}{\partial x} + R_i \tag{1}$$

where, $\dot{N}''_{x,i}$ is the flux of species i and R_i is the rate of electrochemical reaction.

The flux of each dissolved species as the sum of convection, diffusion and migration is given by [8,13]:

$$\dot{N}''_{x,i} = c_i\bar{V} - D_{eff}\frac{\partial c_i}{\partial x} + \frac{t^0_i}{z_iF}i_2 \quad \text{(for positive or negative charge)} \tag{2}$$

$$\dot{N}''_{x,i} = c_0\bar{V} - D_{eff}\frac{\partial c_0}{\partial x} \quad \text{(for solvent)} \tag{3}$$

Using binary electrolyte theory, the mass balance can be expressed as:

$$\varepsilon\frac{\partial c}{\partial t} + \bar{V}\frac{\partial c}{\partial x} - \frac{\partial}{\partial x}\left(\varepsilon^{ex}D\frac{\partial c}{\partial x}\right) - \left[-\frac{s_+}{\upsilon_+nF} - \frac{t^0_+}{\upsilon_+z_+F} + \frac{c}{nF} \times \left(\frac{s_+\bar{V}_e}{\upsilon_+} + \frac{nt^0_+\bar{V}_e}{\upsilon_+z_+} + s_0\bar{V}_0\right)\right]\frac{\partial i_2}{\partial x} = 0 \tag{4}$$

where, $\bar{V}$ represents the convective volume average velocity of the solution [8,13,14]:

$$\bar{V} = -\frac{1}{nF}\left(\frac{s_+\bar{V}_e}{\upsilon_+} + \frac{nt^0_+\bar{V}_e}{\upsilon_+z_+} + s_0\bar{V}_0 + \sum_k^{\text{Solid species}}\frac{s_kM_k}{\rho_k}\right)i_2 \tag{5}$$

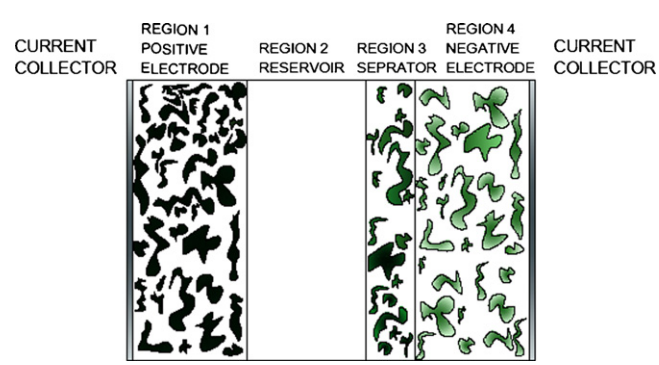

Fig. 1. Schematic of a lead-acid cell structure (not to scale).

Table 1
Simplified model of the lead-acid battery.

Cell component	Governing equations
Positive electrode	$\varepsilon\frac{\partial c}{\partial t}-\frac{\partial}{\partial x}\left(\varepsilon^{\mathrm{ex_{pos}}}D\frac{\partial c}{\partial x}\right)-\left[\left(\frac{3-2t_+^0}{2F}\right)(1-c\bar{V}_e)+\frac{c\bar{V}_0}{F}\right]\frac{\partial i_2}{\partial x}=0$
	$\frac{\partial\varepsilon}{\partial t}-\frac{1}{2F}\left(\frac{M_{\mathrm{PbSO_4}}}{\rho_{\mathrm{PbSO_4}}}-\frac{M_{\mathrm{PbO_2}}}{\rho_{\mathrm{PbO_2}}}\right)\frac{\partial i_2}{\partial x}=0$
	$\frac{i_2}{\varepsilon^{\mathrm{ex_{pos}}}k}+\frac{\partial\phi_2}{\partial x}-\frac{RT}{F}\left(1-2t_+^0\right)\frac{\partial\ln(c)}{\partial x}=0$
	$i_2-\varepsilon^{\mathrm{exm,\,pos}}\sigma_{\mathrm{PbO_2}}\frac{\partial\phi_1}{\partial x}-I=0$
	$\frac{\partial i_2}{\partial x}-a_{\mathrm{max,\,pos}}i_{0,\mathrm{pos,\,ref}}\left(\frac{C}{C_{\mathrm{ini}}}\right)^{y_{\mathrm{pos}}}\left(\frac{\varepsilon-\varepsilon_{o,\mathrm{pos}}}{\varepsilon_{\mathrm{max,\,pos}}-\varepsilon_{0,\mathrm{pos}}}\right)^{\zeta_{\mathrm{pos}}}$
	$\left[\exp\left(\frac{\alpha_{a,\,\mathrm{pos}}F}{RT}(\phi_1-\phi_2-U^0_{\mathrm{PbO_2}})-\exp\left(-\frac{\alpha_{c,\,\mathrm{pos}}F}{RT}\right)(\phi_1-\phi_2-U^0_{\mathrm{PbO_2}})\right)\right]$
	$-C_{\mathrm{dl}}a_{\mathrm{max,\,pos}}\left(\frac{\partial\phi_1}{\partial t}-\frac{\partial\phi_1}{\partial t}\right)=0$
Reservoir	$\frac{\partial c}{\partial t}-\frac{\partial}{\partial x}\left(D\frac{\partial c}{\partial x}\right)=0$
	$\varepsilon=1$
	$\frac{i_2}{\kappa}+\frac{\partial\phi_2}{\partial x}-\frac{RT}{F}(1-2t_+^0)\frac{\partial\ln(c)}{\partial x}=0$
	$\phi_1=0$
	$i_2=I$
Separator	$\varepsilon\frac{\partial c}{\partial t}-\frac{\partial}{\partial x}\left(\varepsilon^{\mathrm{ex_{sep}}}D\frac{\partial c}{\partial x}\right)=0$
	$\varepsilon=\varepsilon_{\mathrm{sep}}$
	$\frac{i_2}{\varepsilon^{\mathrm{ex_{sep}}}\kappa}+\frac{\partial\phi_2}{\partial x}-\frac{RT}{F}(1-2t_+^0)\frac{\partial\ln(c)}{\partial x}=0$
	$\phi_1=0$
	$i_2=I$
Negative electrode	$\varepsilon\frac{\partial c}{\partial t}-\frac{\partial}{\partial x}\left(\varepsilon^{\mathrm{ex_{neg}}}D\frac{\partial c}{\partial x}\right)-\left[\left(\frac{1-2t_+^0}{2F}\right)(1-c\bar{V}_e)\right]\frac{\partial i_2}{\partial x}=0$
	$\frac{\partial\varepsilon}{\partial t}+\frac{1}{2F}\left(\frac{M_{\mathrm{PbSO_4}}}{\rho_{\mathrm{PbSO_4}}}-\frac{M_{\mathrm{Pb}}}{\rho_{\mathrm{Pb}}}\right)\frac{\partial i_2}{\partial x}=0$
	$\frac{i_2}{\varepsilon^{\mathrm{ex_{neg}}}\kappa}+\frac{\partial\phi_2}{\partial x}-\frac{RT}{F}(1-2t_+^0)\frac{\partial\ln(c)}{\partial x}=0$
	$i_2-\varepsilon^{\mathrm{exm,\,neg}}\sigma_{\mathrm{Pb}}\frac{\partial\phi_1}{\partial x}-I=0$
	$\frac{\partial i_2}{\partial x}-a_{\mathrm{max,\,neg}}i_{0,\,\mathrm{neg,\,ref}}\left(\frac{c}{c_{\mathrm{init}}}\right)^{\gamma_{\mathrm{neg}}}\left(\frac{\varepsilon-\varepsilon_{0,\,\mathrm{neg}}}{\varepsilon_{\mathrm{max,\,neg}}-\varepsilon_{0,\,\mathrm{neg}}}\right)^{\zeta_{\mathrm{neg}}}\times\left[\exp\left(\frac{\alpha_{a,\,\mathrm{neg}}F}{RT}(\phi_1-\phi_2-U^0_{\mathrm{Pb}})\right)-\exp\left(-\frac{\alpha_{c,\,\mathrm{neg}}F}{RT}(\phi_1-\phi_2-U^0_{\mathrm{Pb}})\right)\right]-$
	$C_{\mathrm{dl}}a_{\mathrm{max,\,neg}}\left(\frac{\partial\phi_1}{\partial t}-\frac{\partial\phi_2}{\partial t}\right)=0$

In Eq. (5), F is Faraday constant, n is the number of electrons involved in the electrode reaction ($n=2$), $\bar{V}_e$ and $\bar{V}_0$ are the partial molar volumes of electrolyte and solvent that can be calculated from Eqs. (6) and (7), respectively.

$$\bar{V}_e=\frac{M_e}{\rho_e} \tag{6}$$

$$\bar{V}_0=\frac{M_0}{\rho_0} \tag{7}$$

Furthermore, υ_+ is dissociation coefficient of positively charged ions ($\upsilon_+=1$ for a binary electrolyte), z_+ is the charge number of positive ion ($z_+=1$), and s_i is the stoichiometric coefficient of each electrode reaction. For the positive electrode and reservoir, $s_+=-3$, $s_0=2$, $s_{\mathrm{PbSo_4}}=1$, and $s_{\mathrm{Pbo_2}}=-1$. Thus, the convective velocity is simplified to:

$$\bar{V}=-\frac{1}{2F}\left(\frac{M_{\mathrm{PbSO_4}}}{\rho_{\mathrm{PbSO_4}}}-\frac{M_{\mathrm{PbO_2}}}{\rho_{\mathrm{PbO_2}}}-(3-2t_+^0)\bar{V}_e+2\bar{V}_0\right)i_2 \tag{8}$$

For negative electrode and separator, the stoichiometric coefficients are $s_+=-1$, $s_0=0$, $s_{\mathrm{PbSO_4}}=-1$, and $s_{\mathrm{Pb}}=1$. Thus,

$$\bar{V}=\frac{1}{2F}\left(\frac{M_{\mathrm{PbSO_4}}}{\rho_{\mathrm{PbSO_4}}}-\frac{M_{\mathrm{Pb}}}{\rho_{\mathrm{Pb}}}+(1-2t_+^0)\bar{V}_e\right)i_2 \tag{9}$$

The convective velocity is proportional to the ionic current density, i_2. Since the ionic current density is uniform in x axis direction of the reservoir and separator (see Fig. 1), the convective velocity is constant in this direction of these cell components.

By substituting Eqs. (8) or (9) into Eq. (4), the mass balance equation in the positive electrode, reservoir, separator and negative electrode can be expressed as follows [8,13,14].

$$\text{Positive electrode}\quad \varepsilon\frac{\partial c}{\partial t}-\frac{1}{2F}\left(\frac{M_{\mathrm{PbSO_4}}}{\rho_{\mathrm{PbSO_4}}}-\frac{M_{\mathrm{PbO_2}}}{\rho_{\mathrm{PbO_2}}}-(3-2t_+^0)\bar{V}_e+2\bar{V}_0\right)i_2\frac{\partial c}{\partial x}-\frac{\partial}{\partial x}\left(\varepsilon^{\mathrm{ex_{pos}}}D\frac{\partial c}{\partial x}\right)-\left[\left(\frac{3-2t_+^0}{2F}\right)(1-c\bar{V}_e)+\frac{c\bar{V}_0}{F}\right]\frac{\partial i_2}{\partial x}=0 \tag{10}$$

$$\text{Reservoir}\quad \frac{\partial c}{\partial t}-\frac{1}{2F}\left(\frac{M_{\mathrm{PbSO_4}}}{\rho_{\mathrm{PbSO_4}}}-\frac{M_{\mathrm{PbO_2}}}{\rho_{\mathrm{PbO_2}}}-(3-2t_+^0)\bar{V}_e+2\bar{V}_0\right)\times i_2\frac{\partial c}{\partial x}-\frac{\partial}{\partial x}\left(D\frac{\partial c}{\partial x}\right)=0 \tag{11}$$

Table 2
Initial and boundary conditions of the model presented in Table 1.

Cell component	Initial conditions	Boundary conditions
Positive electrode	$c\|_{t=0} = c_{\text{init}}$ $\varepsilon\|_{t=0} = \varepsilon_{\text{max, pos}}$	$\frac{\partial c}{\partial x}\Big\|_{x=0} = 0, \quad \varepsilon^{\text{ex}_{\text{pos}}} \frac{\partial c}{\partial x}\Big\|_{x=l^-_{\text{pos}}} = \frac{\partial c}{\partial x}\Big\|_{x=l^+_{\text{pos}}}$ $\frac{\partial \varepsilon}{\partial x}\Big\|_{x=0} = 0, \quad \frac{\partial \varepsilon}{\partial t}\Big\|_{x=l^-_{\text{pos}}} = \frac{1}{2F}\left(\frac{M_{\text{PbSO}_4}}{\rho_{\text{PbSO}_4}} - \frac{M_{\text{PbO}_2}}{\rho_{\text{PbO}_2}}\right) \frac{\partial i_2}{\partial x}\Big\|_{x=l^-_{\text{pos}}}$ $\frac{\partial \phi_2}{\partial x}\Big\|_{x=0} = 0, \quad \varepsilon^{\text{ex}_{\text{pos}}} \frac{\partial \phi_2}{\partial x}\Big\|_{x=l^-_{\text{pos}}} = \frac{\partial \phi_2}{\partial x}\Big\|_{x=l^+_{\text{pos}}}$ $\frac{\partial \phi_1}{\partial x}\Big\|_{x=l_{pos}} = 0$ $\frac{\partial \phi_1}{\partial x}\Big\|_{x=0} = -\frac{I}{\varepsilon^{\text{exm}_{\text{pos}}}\sigma_{\text{PbO}_2}}$
Reservoir	$c\|_{t=0} = c_{\text{init}}$	$\frac{\partial c}{\partial x}\Big\|_{x=l_{\text{pos}}+l^-_{\text{res}}} = \varepsilon^{\text{ex}_{\text{sep}}} \frac{\partial c}{\partial x}\Big\|_{x=l_{\text{pos}}+l^+_{\text{res}}}$ $\frac{\partial \phi_2}{\partial x}\Big\|_{x=l_{\text{pos}}+l^-_{\text{res}}} = \varepsilon^{\text{ex}_{\text{sep}}} \frac{\partial \phi_2}{\partial x}\Big\|_{x=l_{\text{pos}}+l^+_{\text{res}}}$
Separator	$c\|_{t=0} = c_{\text{init}}$	$\varepsilon^{\text{ex}_{\text{sep}}} \frac{\partial c}{\partial x}\Big\|_{x=l_{\text{pos}}+l_{\text{res}}+l^-_{\text{sep}}} = \varepsilon^{\text{ex}_{\text{neg}}} \frac{\partial c}{\partial x}\Big\|_{x=l_{\text{pos}}+l_{\text{res}}+l^+_{\text{sep}}}$ $\varepsilon^{\text{ex}_{\text{sep}}} \frac{\partial \phi_2}{\partial x}\Big\|_{x=l_{\text{pos}}+l_{\text{res}}+l^-_{\text{sep}}} = \varepsilon^{\text{ex}_{\text{neg}}} \frac{\partial \phi_2}{\partial x}\Big\|_{x=l_{\text{pos}}+l_{\text{res}}+l^+_{\text{sep}}}$
Negative electrode	$c\|_{t=0} = c_{\text{init}}$ $\varepsilon\|_{t=0} = \varepsilon_{\text{max, neg}}$	$\frac{\partial c}{\partial x}\Big\|_{x=l} = 0$ $\frac{\partial \varepsilon}{\partial x}\Big\|_{x=l} = 0$ $\frac{\partial \varepsilon}{\partial t}\Big\|_{x=l_{\text{pos}}+l_{\text{res}}+l_{\text{sep}}} = -\frac{1}{2F}\left(\frac{M_{\text{PbSO}_4}}{\rho_{\text{PbSO}_4}} - \frac{M_{\text{Pb}}}{\rho_{\text{Pb}}}\right) \frac{\partial i_2}{\partial x}\Big\|_{x=l_{\text{pos}}+l_{\text{res}}+l_{\text{sep}}}$ $\phi_1\Big\|_{x=l} = 0, \quad \frac{\partial \phi_1}{\partial x}\Big\|_{x=l_{\text{pos}}+l_{\text{res}}+l_{\text{sep}}} = 0$ $\frac{\partial \phi_1}{\partial x}\Big\|_{x=l} = -\frac{I}{\varepsilon^{\text{exm}_{\text{neg}}}\sigma_{\text{Pb}}}$

Table 3
The list of the model parameters [13].

Parameter	Unit	Positive electrode	Reservoir	Separator	Negative electrode
α_a	–	1.21	–	–	1.55
α_c	–	0.79	–	–	0.45
γ	–	0	–	–	0
ε_0	–	0.3466	–	–	0.3066
ε_{max}	–	0.53	–	–	0.53
ε_{sep}	–	–	–	0.73	–
ζ	–	2	–	–	2
a_{max}	cm^2/cm^3	2.3×10^5	–	–	2.3×10^4
C_{dl}	F/cm^2	2×10^{-5}	–	–	2×10^{-5}
ex	–	1.5	–	3.53	1.5
exm	–	0.5	–	–	0.5
$i_{0,\text{ref}}$	A/cm^2	3×10^{-7}		–	3×10^{-6}
l	μm	700	1760	60	750
$\rho_{\text{H}_2\text{O}}$	g/cm^3	1.03	–	–	–
ρ_{Pb}	g/cm^3	11.34	–	–	–
ρ_{PbO_2}	g/cm^3	9.7	–	–	–
ρ_{PbSO_4}	g/cm^3	6.3	–	–	–
σ_{Pb}	S/cm	–	–	–	4.8×10^4
σ_{PbO_2}	S/cm	80	–	–	–
β	–	0.45 [18]	–	–	0.45 [18]
$\bar{V}_e$	cm^3/mol		45		
$\bar{V}_o$	cm^3/mol		17.5		
C_{init}	mol/m^3		4890		
W	cm		14.4		
h	cm		11.25		
t^0_+	–		0.72		
n	–		2		
T	K		298.15		

Table 4
The list of the model parameters as a function of the electrolyte concentration.

Parameter	Equation	Ref.
Electrolyte diffusion coefficient	$D = 10^{-5}(1.75 + 260c)$	[16]
Electrolyte ionic conductivity	$\kappa = c\exp(6.229 - 133.934c - 16097c^2)$	[16]
Standard electrode potentials	$U^0_{\text{PbO}_2} = 1.628194 + 0.073924\log m + 0.033120\log^2 m - 0.030552\log^3 m + 0.021567\log^4 m$	[19]
	$U^0_{\text{Pb}} = -0.294606 - 0.073595\log m - 0.030432\log^2 m - 0.030552\log^3 m - 0.012045\log^4 m$ $m = 1.00322 \times 10^3 c + 3.55 \times 10^4 c^2 + 2.17 \times 10^6 c^3 + 2.06 \times 10^8 c^4$	

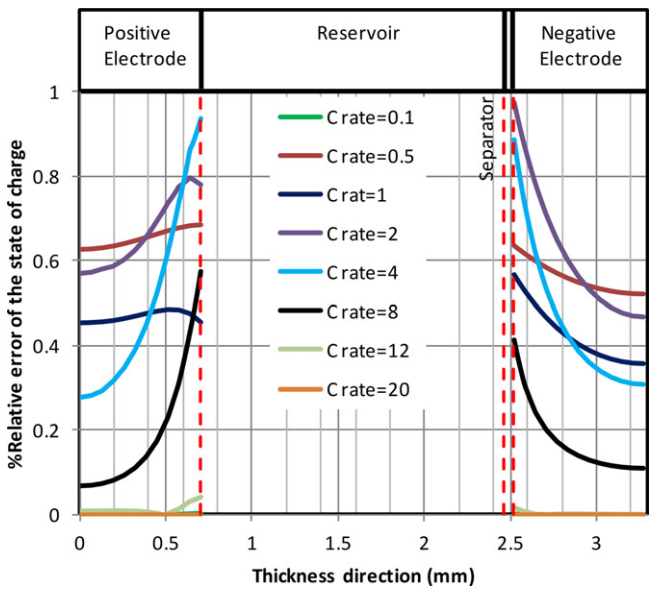

Fig. 2. Modeling error in prediction of the electrode state of charge at the time at which the cell voltage reaches the cut-off voltage of 1.75 V.

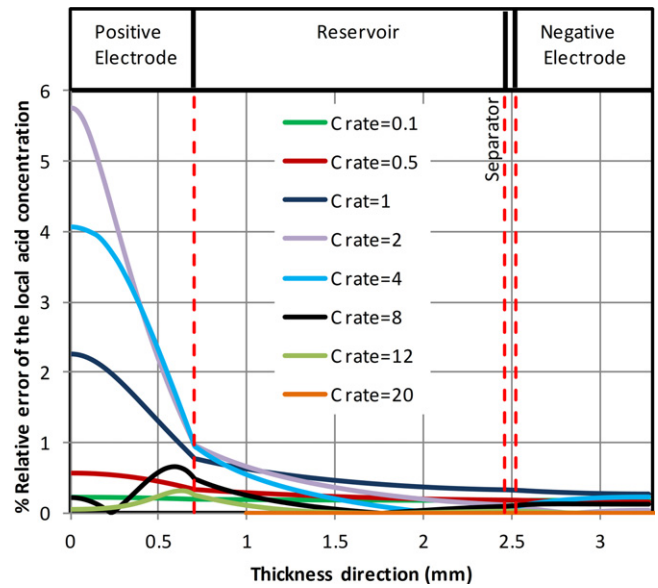

Fig. 3. Modeling error in prediction of the acid concentration at the time at which the cell voltage reaches the cut-off voltage of 1.75 V.

$$\text{Separator}\quad \varepsilon\frac{\partial c}{\partial t}+\frac{1}{2F}\left(\frac{M_{PbSO_4}}{\rho_{PbSO_4}}-\frac{M_{Pb}}{\rho_{Pb}}+(1-2t_+^0)\bar{V}_e\right)i_2\frac{\partial c}{\partial x}-\frac{\partial}{\partial x}\left(\varepsilon^{ex_{sep}}D\frac{\partial c}{\partial x}\right)=0 \tag{12}$$

$$\text{Negative electrode}\quad \varepsilon\frac{\partial c}{\partial t}+\frac{1}{2F}\left(\frac{M_{PbSO_4}}{\rho_{PbSO_4}}-\frac{M_{Pb}}{\rho_{Pb}}+(1-2t_+^0)\bar{V}_e\right)\times i_2\frac{\partial c}{\partial x}-\frac{\partial}{\partial x}\left(\varepsilon^{ex_{neg}}D\frac{\partial c}{\partial x}\right)-\left[\left(\frac{1-2t_+^0}{2F}\right)(1-c\bar{V}_e)\right]\frac{\partial i_2}{\partial x}=0 \tag{13}$$

Obviously, if the convective term can be neglected, the mass balance Eqs. (10)–(13) are significantly simplified. The simplified model equations and the corresponding initial and boundary conditions are presented in Tables 1 and 2, respectively. In Table 1, the electrode kinetics is presented by Butler-Volmer equation and the effect of electrical double layer is included in the electrode kinetics model.

In this study, the battery performance is demonstrated in the Ragone plot. In this plot, the x and y axes are the battery specific power and energy, respectively. The specific energy and power are calculated from the following equations:

$$E_{cell}=\frac{1}{\omega_{cell}}\int_0^{t_{discharge}} i_{cell}v_{cell}dt \tag{14}$$

$$P_{cell}=\frac{E_{cell}}{t_{discharge}} \tag{15}$$

where, $t_{discharge}$ is the cell discharge time to reach a given cut-off voltage and ω_{cell} is the total mass per unit area of the battery, which can be calculated from Eq. (14).

$$\begin{aligned}\omega_{cell}=&\ \rho_{PbO_2}(1-\varepsilon_{pos})l_{pos}+\rho_e\varepsilon_{pos}l_{pos}+\rho_e l_{Res}+\rho_{sep}(1-\varepsilon_{sep})l_{sep}\\&+\rho_e\varepsilon_{sep}l_{sep}+\rho_{Pb}(1-\varepsilon_{neg})l_{neg}+\rho_e\varepsilon_{neg}l_{neg}\\&+\beta_{pos}\rho_{PbO_2}(1-\varepsilon_{pos})l_{pos}+\beta_{neg}\rho_{Pb}(1-\varepsilon_{neg})l_{neg}\end{aligned} \tag{16}$$

In lead-acid batteries, the electrode state of charge is a function of the electrode porosity and can be obtained from the following equation:

$$soc=\left(\frac{\varepsilon-\varepsilon_0}{\varepsilon_{max}-\varepsilon_0}\right) \tag{17}$$

3. Results and discussions

The lead-acid battery model with full mass transfer mechanisms – including convection, migration and diffusion – employed in the present work is a well-established model and has been extensively utilized in the literature [8,13,14]. The maximum relative error of battery voltage, determined from this model as a function of time is 4.9% compared to the experimental data during discharge [14]. The low maximum relative error of simulated battery voltage demonstrates that the mentioned model is capable of predicting the battery performance accurately. Moreover, this model can be employed to determine the cell internal variables such as the local electrode state of charge and local acid concentration. To make sure of the accuracy of the local porosity and local acid concentration, they were calculated from the present model simulation

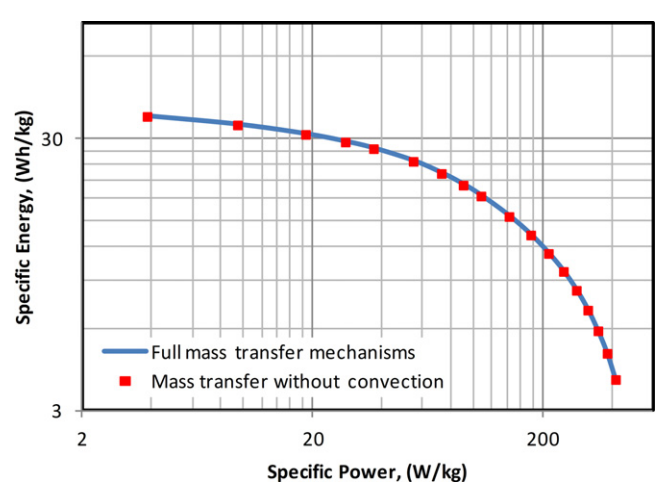

Fig. 4. Modeling error in prediction of the cell specific power and energy.

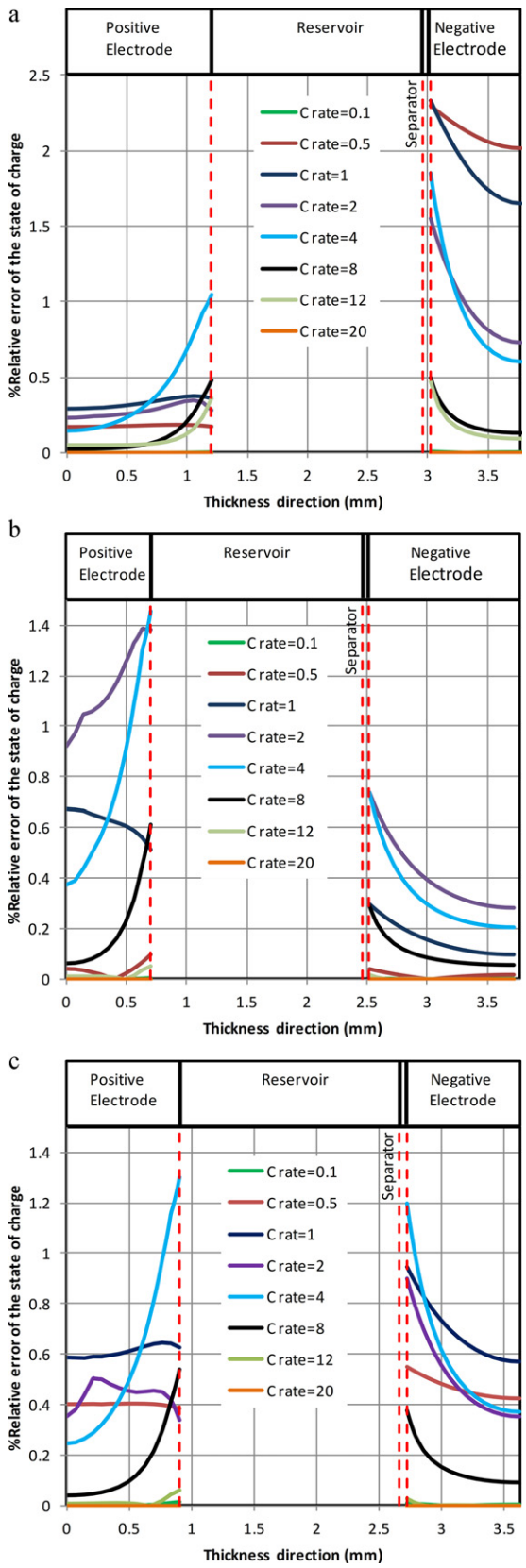

Fig. 5. Modeling error in prediction of the electrode state of charge at the time at which the cell voltage reaches the cut-off voltage of 1.75 V for a cell with (a) a thick positive electrode ($l_{pos} = 700\,\mu m$, $l_{neg} = 1200\,\mu m$), (b) a thick negative electrode ($l_{pos} = 700\ \mu m$, $l_{neg} = 1200\,\mu m$), and (c) the positive and negative electrode thicknesses of 900 μm.

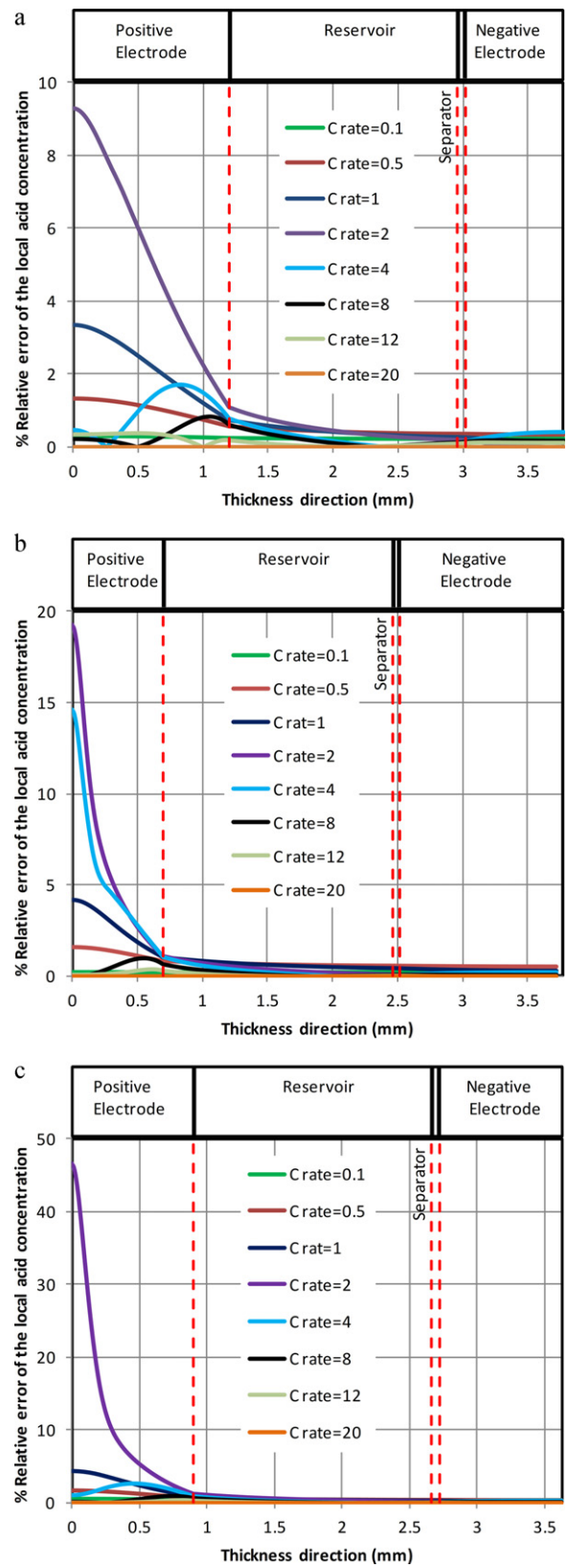

Fig. 6. Modeling error in prediction of the acid concentration at the time at which the cell voltage reaches the cut-off voltage of 1.75 V for a cell with (a) a thick positive electrode ($l_{pos} = 1200\,\mu m$, $l_{neg} = 750\,\mu m$), (b) a thick negative electrode ($l_{pos} = 700\,\mu m$, $l_{neg} = 1200\,\mu m$), and (c) the positive and negative electrode thicknesses of 900 μm.

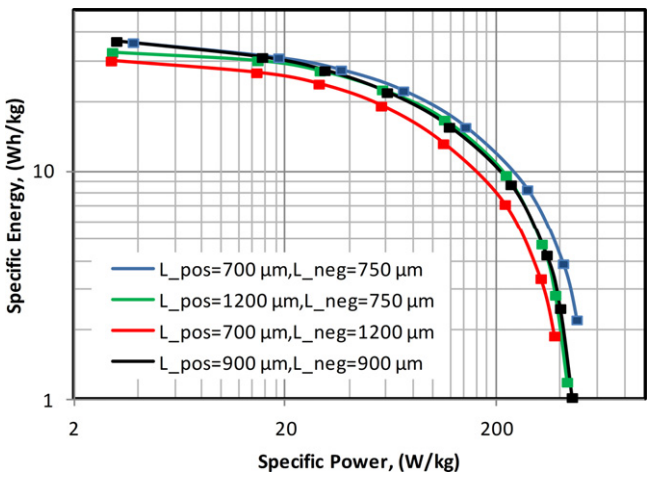

Fig. 7. Modeling error in prediction of the specific power and energy of the cells with various electrode thicknesses (Curves: the model that considers full mass transfer equations; Dots: the model in which the convective mass transfer has been neglected).

and compared with those represented in Ref. [14]. The maximum relative error of the local porosity and the local acid concentration in the present simulation with respect to those shown in Ref. [14] was less than 1%. Hence, the electrode state of charge calculated from Eq. (17) and local acid concentration obtained from the present simulation could be reliable for our investigations.

To study the convective mass transfer effect on the modeling accuracy, the computer simulation results obtained from the model that considers full mass transfer equations and a model in which the convective mass transfer has been neglected (see Table 1) are compared. For this purpose, the results obtained from the former model is considered as the base results; and the relative error of the results obtained from the latter model with respect to the base results is determined. For both models, the input parameters listed in Table 3 are employed, which is based on the manufacturer data for a commercialized sealed lead-acid battery (VARTA L2 400-60 Ah) [14]. In addition, Table 4 represents the model concentration dependent parameters. The cell cut-off voltage is 1.75 V [17] for all the results presented in this paper.

Fig. 2 depicts the modeling error for prediction of the local electrode state of charge when the convective phenomenon is neglected from mass transfer equations. As shown in this figure, the modeling error at the interface of the positive electrode and reservoir is greater than that at the interface of the positive electrode and current collector. The modeling error at the interface of the negative electrode and separator is also greater than that at the interface of the negative electrode and current collector. The modeling error is below 0.05% for c-rate < 0.1 and c-rate > 12. The maximum error for all c-rates investigated (C/10 – 20C) is below 1%. Thus, the convective mass transfer phenomenon has no significant effect on prediction of the electrodes state of charge of the cell studied.

Fig. 3 illustrates the modeling error for prediction of the local acid concentration associated with neglecting convective mass transfer. The convection has more effect on the local acid concentration in comparison with the local electrode state of charge. Nevertheless, for the cell studied, the maximum modeling error is estimated to be around 6% at c-rate = 2 that happens at the interface of the positive electrode and current collector. Furthermore, the modeling error is less than 1% across the reservoir, separator, and negative electrode for all c-rates investigated. Hence, the modeling error for prediction of the local acid concentration is negligible at

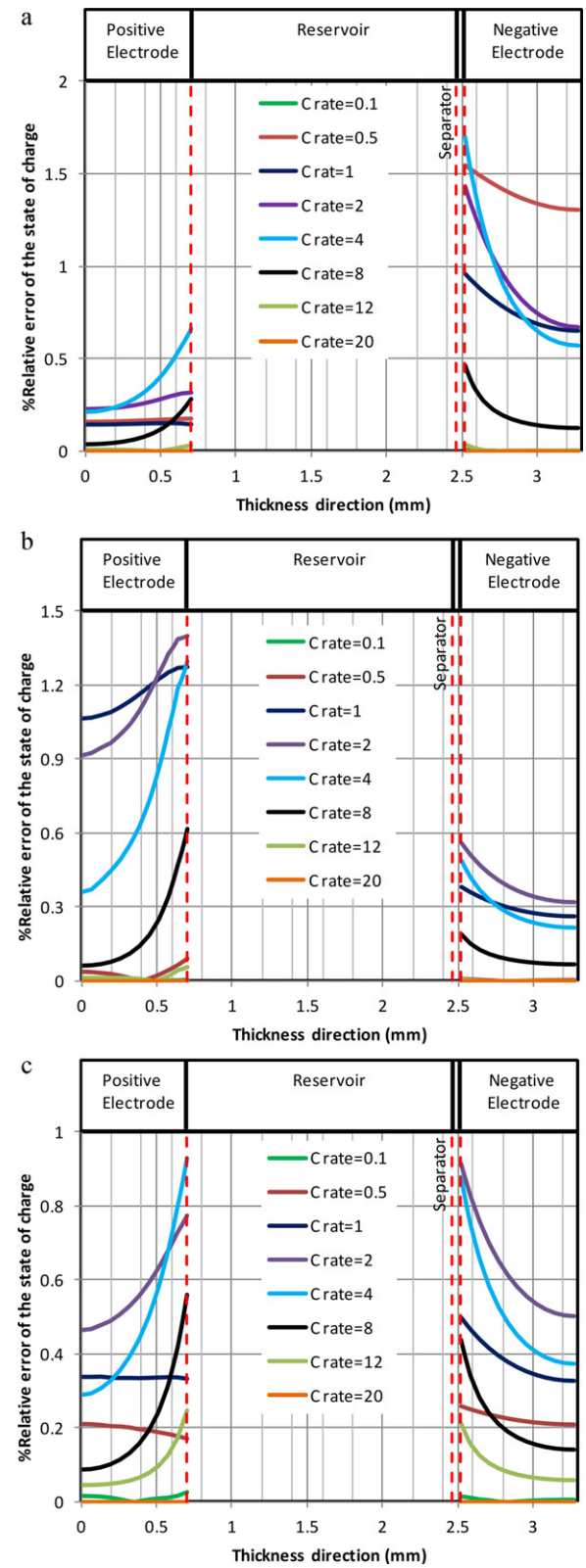

Fig. 8. Modeling error in prediction of the electrode state of charge at the time at which the cell voltage reaches the cut-off voltage of 1.75 V for a cell with the positive and negative electrode initial porosities of (a) 0.65 and 0.52 (b) 0.52 and 0.65 (c) 0.65 and 0.65, respectively.

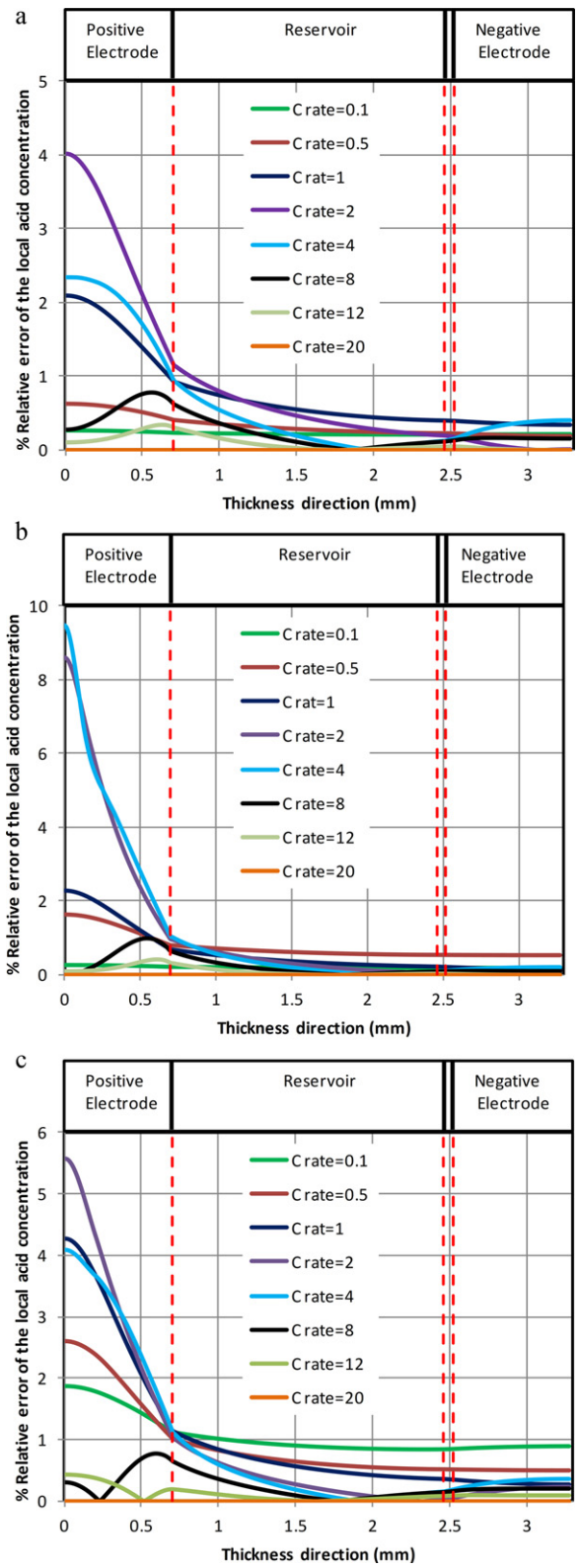

Fig. 9. Modeling error in prediction of the acid concentration at the time at which the cell voltage reaches the cut-off voltage of 1.75 V for a cell with the positive and negative electrode initial porosities of (a) 0.65 and 0.52 (b) 0.52 and 0.65 (c) 0.65 and 0.65, respectively.

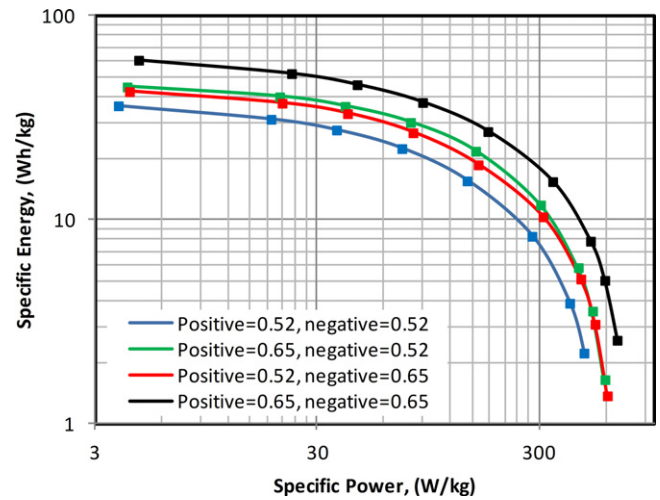

Fig. 10. Modeling error in prediction of the specific power and energy of the cells with various electrode initial porosities (Curves: the model that considers full mass transfer equations; Dots: the model in which the convective mass transfer has been neglected).

reservoir, separator, and negative electrode. This statement is valid for the positive electrode operated at c-rate < 0.5 or c-rate > 8.

Fig. 4 demonstrates the Ragone plot for the computer simulation based on the model that considers full mass transfer equations (blue curve) and the model that the convective mass transfer has been neglected from the mass transfer equations (red dots). The results for the cell studied indicated that the modeling error for predicting the cell specific power and energy at various c-rates is less than 0.8% if the convective mass transfer is neglected.

To generalize the results, a sensitivity analysis is conducted to determine the modeling error for the cells with various design parameters such as the electrode thickness, electrode porosity, and initial acid concentration.

3.1. *Effect of the electrode thickness*

The cell studied so far has the positive and negative electrode thicknesses of 700 μm and 750 μm, respectively. To evaluate the effect of the electrode thickness on the modeling error associated with neglecting the convective mass transfer, three cells with various electrode thicknesses are simulated. The first cell has a thick positive electrode ($l_{pos} = 1200\,\mu m$, $l_{neg} = 750\,\mu m$), the second cell has a thick negative electrode ($l_{pos} = 700\,\mu m$, $l_{neg} = 1200\,\mu m$), and the third cell has the positive and negative electrode thicknesses of 900 μm. The other model design parameters are assumed to be constant.

As shown in Fig. 5a, the maximum modeling error for predicting the local electrode state of charge of the cell with a thick positive electrode is less than 2.4% and happens at the interface of the negative electrode and separator. This error is less than 1.5% for the cell with a thick negative electrode and happens at the interface of the positive electrode and reservoir (see Fig. 5b). For the cell with the positive and negative electrode thicknesses of 900 μm, the maximum modeling error is less than 1.4% (see Fig. 5c).

As shown in Fig. 6a, the maximum modeling error for predicting the local acid concentration for the cell with a thick positive electrode is around 9%. This maximum error is around 19% for the cell with a thick negative electrode (see Fig. 6b) and 47% for the cell with the positive and negative electrode thicknesses of 900 μm (see Fig. 6c). All of these maximum errors happen at the interface of the positive electrode and current collector. The modeling error is less than 2% across the reservoir, separator, and negative electrode for

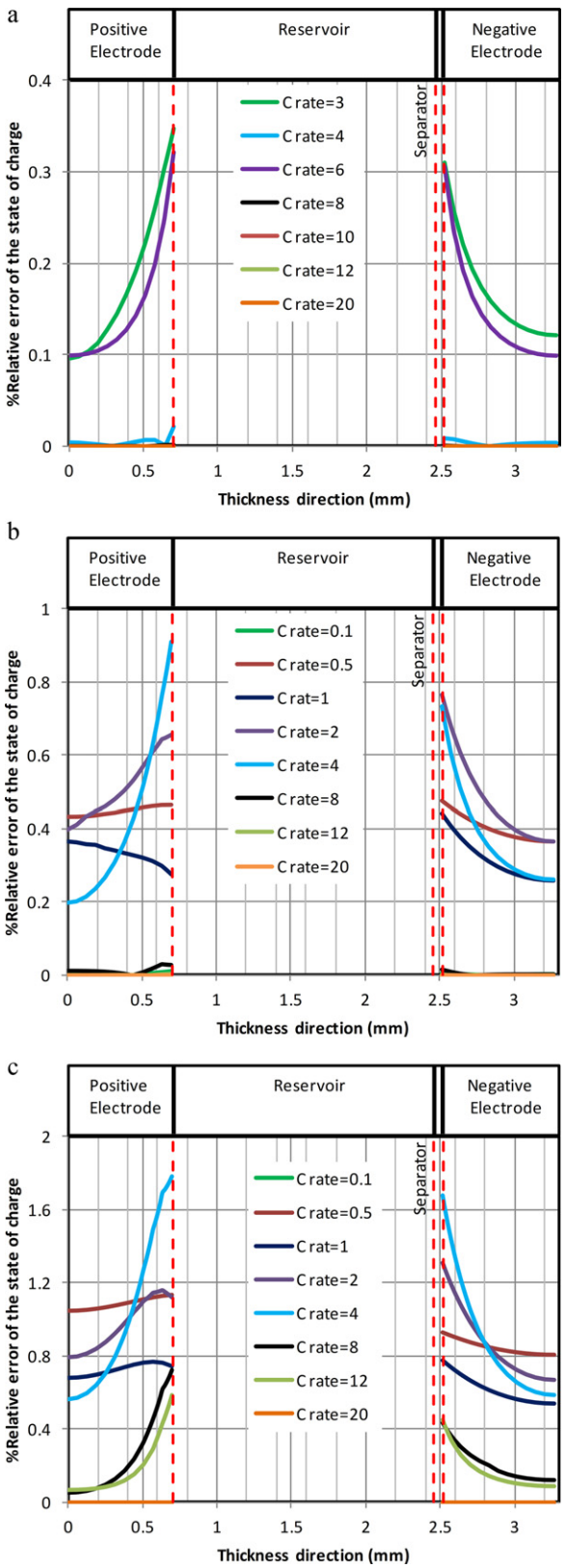

Fig. 11. Modeling error in prediction of the electrode state of charge at the time at which the cell voltage reaches the cut-off voltage of 1.75 V for a cell with the initial acid concentration of (a) 3 M (b) 4 M (c) 6 M.

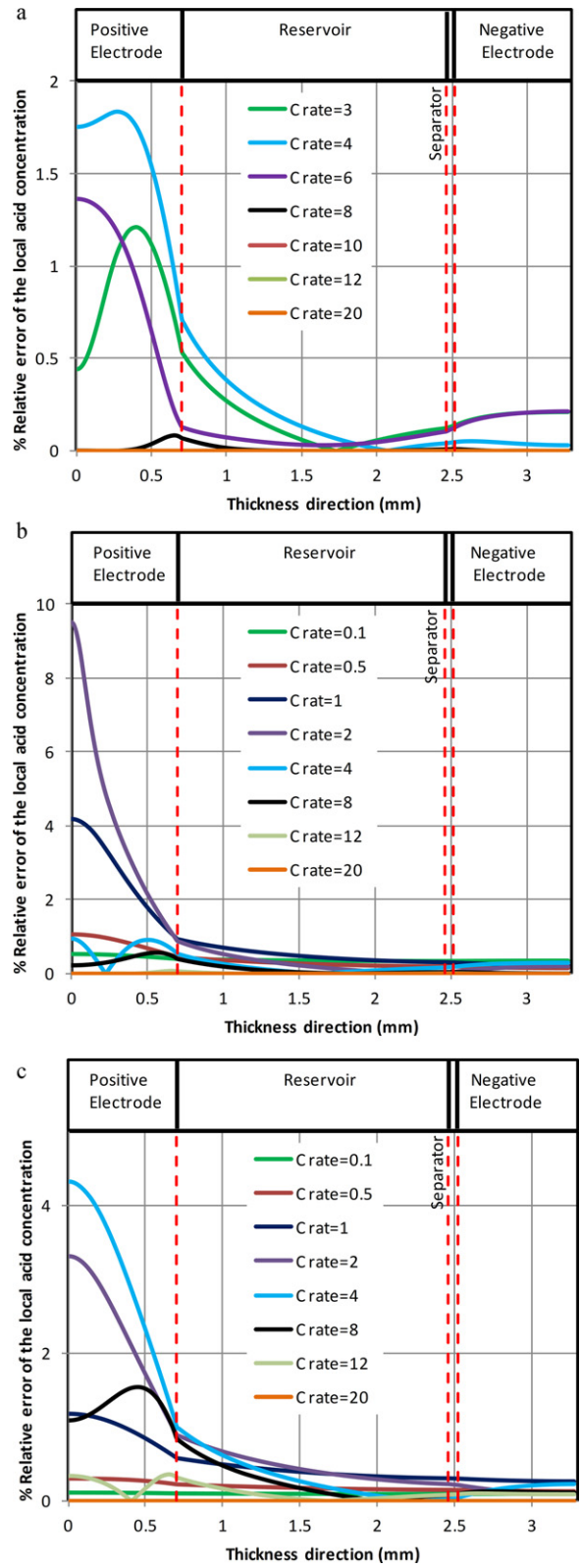

Fig. 12. Modeling error in prediction of the acid concentration at the time at which the cell voltage reaches the cut-off voltage of 1.75 V for a cell with the initial acid concentration of (a) 3 M (b) 4 M (c) 6 M.

all c-rates and thicknesses investigated. This statement is valid for the positive electrode operated at c-rate < 0.5 or c-rate > 8.

The Ragone plot for the cells with various electrode thicknesses is depicted in Fig. 7. Our studies show that the model with the neglected convective mass transfer can predict the specific power and energy of the lead-acid cells with a relative error of less than 1%.

3.2. Effect of the electrode initial porosity

Both electrodes of the cell studied had the initial porosity of 0.52. To evaluate the effect of the electrode initial porosity on the modeling error due to neglecting the convective mass transfer, three cells with different initial porosities are examined. The first cell has the positive and negative electrode initial porosities of 0.65 and 0.52, respectively. These values for the second cell are 0.52 and 0.65, respectively. The third cell has the positive and negative electrode initial porosities of 0.65. The other model design parameters were assumed to be constant and independent of the electrode initial porosity.

As shown in Fig. 8a, the maximum error for prediction of the local electrode state of charge of the first cell is less than 1.6%, which takes place at the interface of the negative electrode and separator. This error is less than 1.5% for the second cell and happens at the interface of the positive electrode and reservoir (see Fig. 8b). For the third cell, the maximum modeling error is less than 0.9% (see Fig. 8c).

As shown in Fig. 9a, the maximum error associated with prediction of the local acid concentration for the cell with the positive and negative electrode initial porosities of 0.65 and 0.52, respectively, is around 4%. This maximum error is around 9.5% for the cell with the positive and negative electrode initial porosities of 0.52 and 0.65, respectively (see Fig. 9b), and less than 6% for the cell with the positive and negative electrode initial porosities of 0.65 (see Fig. 9c). All of these maximum errors occur at the interface of the positive electrode and current collector. The modeling error is less than 2% across the reservoir, separator, and negative electrode for all c-rates and porosities investigated. This statement is valid for the positive electrode operated at c-rate < 0.1 or c-rate > 8.

The Ragone plot for the cells with various electrode initial porosities is illustrated in Fig. 10. Our studies confirm that the model with the neglected convective mass transfer can predict the specific power and energy of the lead-acid cells with various initial porosities with a relative error of less than 1%.

3.3. Effect of the initial acid concentration

The cell studied so far has the initial acid concentration of 4.89 M. To evaluate the effect of this concentration on the modeling error associated with neglecting the convective mass transfer, three cells with various initial acid concentrations are studied. The first cell has an initial acid concentration of 3 M. This value for the second and third cells are 4 M and 6 M, respectively. The other model design parameters are assumed to be constant during the sensitivity analysis. In case of the initial acid concentration of 3 M, it was impossible to test c-rates below 3 because the electrolyte was depleted and limited the cell operation.

As shown in Fig. 11a, the maximum modeling error for prediction of the local electrode state of charge of the cell with initial acid concentration of 3 M is less than 0.4%. This maximum error is less than 0.9% (see Fig. 11b) and 1.8% (see Fig. 11c) for the cells with the initial acid concentrations of 4 M and 6 M, respectively. All of these maximum errors take place at the interface of the positive electrode and current collector.

As shown in Fig. 12a, the maximum error for prediction of the local acid concentration for the cell with the initial acid concentration of 3 M is less than 2% and occurs in the positive electrode. This maximum error is around 10% (see Fig. 12b) and 5% (see Fig. 12c) for the cells with initial acid concentrations of 4 M and 6 M, respectively. In case of the initial acid concentration of 4 M and 6 M, the maximum errors happen at the interface of the positive electrode and current collector. The modeling error is less than 2% across the reservoir, separator, and negative electrode for all c-rates and initial acid concentrations investigated. This statement is valid for the positive electrode operated at c-rate < 0.5 or c-rate > 8.

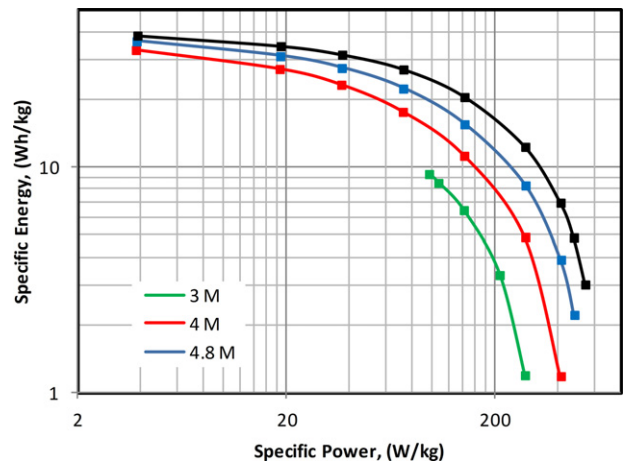

Fig. 13. Modeling error in prediction of the specific power and energy of the cell with various initial acid concentrations (Curves: the model that considers full mass transfer equations; Dots: the model in which the convective mass transfer has been neglected).

The Ragone plot for the cells with various initial acid concentrations is demonstrated in Fig. 13. Our studies show that the model with the neglected convective mass transfer can predict the specific power and energy of the lead-acid cells with various initial acid concentrations with a relative error of less than 1%.

4. Conclusions

The computer simulation results obtained from a model that considers full mass transfer equations and a model in which the convective mass transfer has been neglected were compared. The aim of this study was to investigate the effect of convective mass transfer phenomenon on the lead-acid battery performance. For this purpose, a comprehensive study was conducted at various battery operating conditions and design parameters – including the electrode thickness, electrode initial porosity, and initial acid concentration – to quantify the effect of this phenomenon on the battery performance. The results indicated that the maximum modeling error for prediction of the local electrode state of charge is less than 2.4% for the cells studied. Thus, the convective mass transfer phenomenon has no significant effect on prediction of the electrode state of charge. The convective mass transfer may significantly affect the local acid concentration in the positive electrode. The maximum modeling error for prediction of this concentration may be around 50%. Of course, the modeling error for prediction of this concentration at reservoir, separator and negative electrode was less than 2% for all the cell design and operating conditions investigated. This statement is valid for the positive electrode of the cells operated at c-rates less than 0.1 or more than 8. The results revealed that the modeling error for prediction of the specific power and energy of the cells studied is less than 1%.

As a remarkable result, the convective mass transfer phenomenon can be neglected in modeling lead-acid batteries if the objective of the study is the prediction of the battery specific power and energy or electrode state of charge. In this condition, an

improvement in terms of the model simplification and reduction in the computational cost can be achieved. Of course, this phenomenon cannot be neglected if the objective is the prediction of the acid concentration in the positive electrode of lead-acid cells operated at c-rates between 0.1 and 8.

Acknowledgments

The authors gratefully acknowledge the support provided by Mitacs Elevate, Ryerson University and University of Waterloo.

References

[1] T.V. Nguyen, R.E. White, A mathematical model of a hermetically sealed lead-acid cell, Electrochimica Acta 38 (1993) 935.
[2] A. Tenno, R. Tenno, T. Suntio, Charge–discharge behaviour of VRLA batteries: model calibration and application for state estimation and failure detection, Journal of Power Sources 103 (2001) 42.
[3] V. Esfahanian, F. Torabi, A. Mosahebi, An innovative computational algorithm for simulation of lead-acid batteries, Journal of Power Sources 176 (2008) 373.
[4] M. Cugnet, B.Y. Liaw, Effect of discharge rate on charging a lead-acid battery simulated by mathematical model, Journal of Power Sources 196 (2011) 3414.
[5] J. Euler, Porendimensionen und Oberflächenkapazität von Braunstein, Electrochimica Acta 4 (1961) 27.
[6] K. Micka, I. Rousar, Theory of porous electrodes – XI. The positive plate of the lead-acid battery, Electrochimica Acta 18 (1973) 629.
[7] W.H. Tiedemann, J. Newman, Battery design and optimization: mathematical modeling of the lead-acid cell, in: The Electrochemical Society Softbound Proceedings Series, Princeton, NJ, 1979, p. 23.
[8] H. Gu, T.V. Nguyen, R.E. White, A mathematical model of a lead acid cell, Journal of the Electrochemical Society 134 (1987) 2953.
[9] P. Ekdunge, D. Simonsson, The discharge behavior of the porous lead electrode in the lead-acid battery. II. Mathematical model, Journal of Applied Electrochemistry 19 (1989) 136.
[10] E.C. Dimpault-Darcy, T.V. Nguyen, R.E. White, A two-dimensional mathematical model of a porous lead dioxide electrode in a lead-acid cell, Journal of the Electrochemical Society 135 (1988) 278.
[11] S.C. Kim, Won H. Hong, Analysis of the discharge performance of a flooded lead/acid cell using mathematical modeling, Journal of Power Sources 77 (1999) 74.
[12] J. Landfors, D. Simonsson, A. Sokirko, Mathematical modeling of a lead/acid cell with immobilized electrolyte, Journal of Power Sources 55 (1995) 217.
[13] V. Boovaragavan, R.N. Methakar, V. Ramadesigan, V.R. Subramanian, A mathematical model of the lead-acid battery to address the effect of corrosion, Journal of the Electrochemical Society 156 (2009) A854.
[14] M. Cugnet, S. Laruelle, S. Grugeon, B. Sahut, J. Sabatier, J. Tarascon, A. Oustaloup, A mathematical model for the simulation of new and aged automotive lead-acid batteries, Journal of the Electrochemical Society 156 (2009) A974.
[15] B. Culpin, D.A.J. Rand, Failure modes of lead/acid batteries, Journal of Power Sources 36 (1991) 415.
[16] J.S. Newman, Electrochemical Systems, 3rd ed., Wiley Interscience, Hoboken, NJ, 2004.
[17] Sealed Lead-Acid Handbook, Panasonic, 1999, 16.
[18] Yu. Kamenev, A. Kiselevich, E. Ostapenko, Evaluation of criteria for design of current collectors of the lead-acid battery, Journal of Power Sources 110 (2002) 133.
[19] H. Bode, Lead-Acid Batteries, John Wiley & Sons, New York, 1977.